ACS Pharmacology & Translational Science

pubs.acs.org/ptsci

Article

Novel Fluorescence-Based High-Throughput FLIPR Assay Utilizing Membrane-Tethered Genetic Calcium Sensors to Identify T-Type Calcium Channel Modulators

Yan-Ling Zhang, Sean P. Moran, Andrew Allen, David Baez-Nieto, Qihong Xu, Lei A. Wang, William E. Martenis, Joshua R. Sacher, Jennifer P. Gale, Michel Weïwer, Florence F. Wagner, and Jen Q. Pan*

Cite This: *ACS Pharmacol. Transl. Sci.* 2022, 5, 156−168

Read Online

ACCESS | Metrics & More | Article Recommendations | Supporting Information

ABSTRACT: T-type voltage-gated Ca^{2+} channels have been implicated in many human disorders, and there has been increasing interest in developing highly selective and potent T-type Ca^{2+} channel modulators for potential clinical use. However, the unique biophysical properties of T-type Ca^{2+} channels are not conducive for developing high-throughput screening (HTS) assays to identify modulators, particularly potentiators. To illustrate, T-type Ca^{2+} channels are largely inactivated and unable to open to allow Ca^{2+} influx at −25 mV, the typical resting membrane potential of the cell lines commonly used in cellular screening assays. To address this issue, we developed cell lines that express $K_{ir}2.3$ channels to hyperpolarize the membrane potential to −70 mV, thus allowing T-type channels to return to their resting state where they can be subsequently activated by membrane depolarization in the presence of extracellular KCl. Furthermore, to simplify the HTS assay and to reduce reagent cost, we stably expressed a membrane-tethered genetic calcium sensor, GCaMP6s-CAAX, that displays superior signal to the background compared to the untethered GCaMP6s or the synthetic Ca^{2+} sensor Fluo-4AM. Here, we describe a novel GCaMP6s-CAAX-based calcium assay utilizing a high-throughput fluorometric imaging plate reader (Molecular Devices, Sunnyvale, CA) format that can identify both activators and inhibitors of T-type Ca^{2+} channels. Lastly, we demonstrate the utility of this novel fluorescence-based assay to evaluate the activities of two distinct G-protein-coupled receptors, thus expanding the use of GCaMP6s-CAAX to a wide range of applications relevant for developing cellular assays in drug discovery.

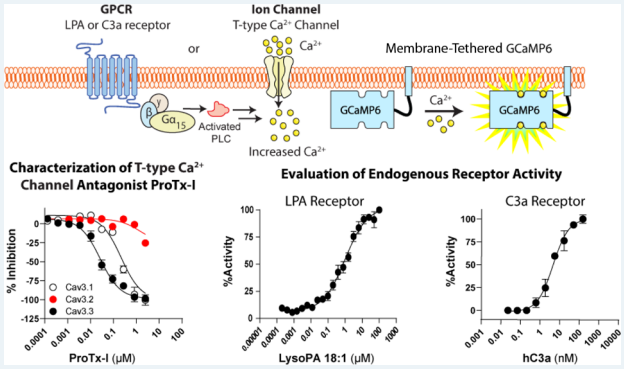

KEYWORDS: *T-type calcium channel, GCaMP6, high-throughput, electrophysiology, fluorometric imaging plate reader, drug discovery*

INTRODUCTION

Voltage-gated calcium channels (VGCCs) provide the primary pathway for calcium (Ca^{2+}) ions to enter excitable cells by allowing rapid and selective Ca^{2+} entry upon membrane depolarization.[1,2] By transducing natural voltage transients, such as action potentials, into intracellular Ca^{2+} transients, voltage-gated Ca^{2+} channels not only contribute to active membrane properties such as Ca^{2+} spikes and dendritic information integration[3,4] but also underlie many cellular functions including neurotransmitter release, neurite outgrowth, cell survival, hormone release, and gene expression.[5−7]

The functional core of the VGCC is composed of the $Ca_V\alpha_1$ subunit, which contains the ion pore, gating mechanism, and toxin-binding domains, and consists of four homologous transmembrane domains (I−IV), cytoplasmic amino- and carboxyl-termini, and intracellular loops connecting each transmembrane domain.[2,8] Ten genes encode $Ca_V\alpha_1$ subunits in humans and are divided into three major subgroups based on structural, functional, and pharmacological similarities.[9] Four genes encode Ca_V1 L-type Ca^{2+} channels, three genes encode Ca_V2 Ca^{2+} channels, and three genes encode Ca_V3 T-type Ca^{2+} channels.[1,10,11]

The T-type α_1 subunits lack the structural motif that mediates the interaction with auxiliary $Ca_V\beta$ subunits[12] that are common to Ca_V1 and Ca_V2 channels. As such, T-type Ca^{2+} channel properties can be fully reconstituted with the α_1 subunit alone in heterologous expression systems, whereas

Received: October 30, 2021
Published: February 25, 2022

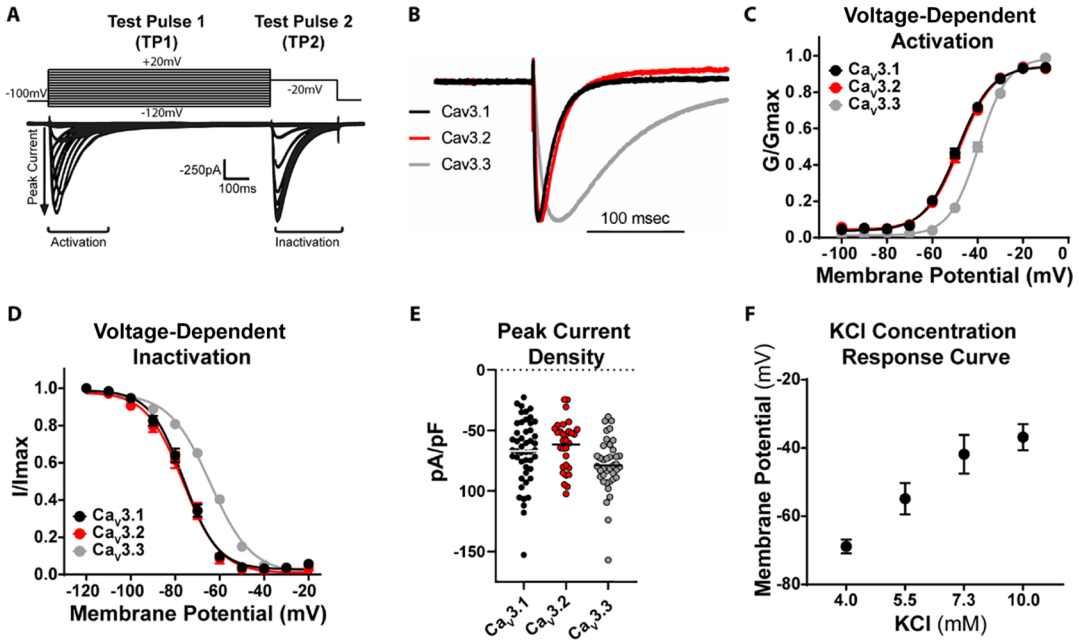

Figure 1. Biophysical properties of HEK293 cells stably expressing $Ca_V3.1$, $Ca_V3.2$, or $Ca_V3.3$ T-type channels using high-throughput in vitro electrophysiology. (A) The current−voltage (*IV*) protocol consists of a sustained depolarization of 1 s from −120 to +20 mV at 10 mV increments (TP1), followed by a voltage step of 300 ms to −20 mV (TP2). The Ca^{2+} currents from the TP1 protocol (activation) were used to construct the "voltage-dependent activation" curve. Ca^{2+} currents from the TP2 protocol (inactivation) were used to establish the "voltage-dependent inactivation" curve. (B) Sample T-type Ca^{2+} currents are shown for $Ca_V3.1$ (black), $Ca_V3.2$ (red), and $Ca_V3.3$ (gray) normalized to the peak current. (C) Voltage-dependent activation curves. $V_{1/2\text{-activation}}$ (voltage at which 50% of the channels are activated) = −48.76 mV (n = 47 cells), −47.96 mV (n = 31 cells), and −39.53 mV (n = 38 cells) for $Ca_V3.1$, $Ca_V3.2$, and $Ca_V3.3$, respectively. (D) Voltage-dependent inactivation curves. $V_{1/2\text{-inactivation}}$ (voltage at which 50% of the channels are inactivated) = −76.30 mV (n = 47 cells), −76.59 mV (n = 31 cells), and −64.42 mV (n = 38 cells) for $Ca_V3.1$, $Ca_V3.2$, and $Ca_V3.3$, respectively. (E) Averaged peak current density of 67.06 ± 3.84 pA/pF (n = 48 cells), −61.60 ± 3.66 pA/pF (n = 31 cells), and −78.80 ± 3.60 pA/pF (n = 39 cells) for $Ca_V3.1$, $Ca_V3.2$, and $Ca_V3.3$, respectively. Data are expressed as mean ± SEM. (F) KCl-induced changes in membrane potentials were recorded from HEK293 cells expressing $K_{ir}2.3$ and $Ca_V3.3$ measured by whole-cell patch clamp electrophysiology (n = 6−7 cells per treatment). Data are expressed as mean ± SEM.

$Ca_V1/2$ Ca^{2+} channel α_1 subunits require the coexpression of auxiliary subunits ($\alpha_2\delta$, β, and γ) that facilitate channel trafficking to the membrane surface for expression.[2,11] While Ca_V1 and Ca_V2 channels require high-threshold depolarizations for activation (typically more than 30 mV), much smaller depolarizations activate Ca_V3 T-type Ca^{2+} channels.[13−15] T-type currents inactivate rapidly (T for transient) and have a small single-channel conductance of 8−12 pS in 100 mM Ba^{2+}.[16] Ca_V3 T-type Ca^{2+} channels have overlapping voltage-dependent activation and inactivation curves, displaying "window currents" where a large fraction of the channels are inactivated, but a small fraction of the channels remain constitutively open at physiological resting membrane potentials.[2] T-type Ca^{2+} channels also close slower from the open state compared to the $Ca_V1/2$ families, allowing large amounts of Ca^{2+} influx upon repolarization to trigger membrane depolarization. These unique biophysical properties of the T-type Ca^{2+} channels produce Ca^{2+} influx during repolarizations that underlie the rhythmic rebound firing of thalamic neurons in the brain and of pacemaker cells within the heart.[9]

Human genetics has implicated all three genes encoding T-type Ca^{2+} channel α_1 subunits in neurological and neuropsychiatric disorders.[17] Rare mutations of *CACNA1G*, the gene encoding the $Ca_V3.1$ α_1 subunit, are associated with severe developmental deficits linked to spinocerebellar ataxia,[18,19] idiopathic generalized epilepsy,[20] and cerebellar atrophy[21] and are thought to be a modifier of epilepsy associated with *SCN2A*.[22] Variants of *CACNA1H*, the gene encoding the $Ca_V3.2$ α_1 subunit, represent susceptibility alleles involved in the pathogenesis of a childhood absence epilepsy.[23] Furthermore, patients with *CACNA1H* loss of function mutations are found to be resistant to pain perception, thus serving as the biological basis for targeting $Ca_V3.2$ in pain management.[24] More recently, gain-of-function mutations in *CACNA1I*, the gene encoding the $Ca_V3.3$ α_1 subunit, have been implicated in neurodevelopmental disorders.[25] Interestingly, several clinical drugs have been found to block T-type Ca^{2+} channels,[2] including the antihypertensive agent mibefradil (withdrawn from the market due to potential off-target drug−drug interactions[26]), certain neuroleptics,[27] and anticonvulsants.[28] Overall, these data support that the selective inhibition of T-type Ca^{2+} channels may have a wide range of therapeutic potentials.

While selectively blocking T-type Ca^{2+} channels are thought to be therapeutically beneficial for several disorders,[21,24,25] emerging evidence suggests that enhancing T-type Ca^{2+} channel function may also provide therapeutic benefit. For example, protein-truncating mutations of *CACNA1G* confer risk for schizophrenia[29] and *CACNA1I* has been implicated in schizophrenia risk.[30] While the exact mechanism underlying *CACNA1I* in schizophrenia risk is unknown, de novo variants of *CACNA1I* derived from schizophrenia patients have been found to reduce channel current density.[30,31] These studies implicate loss of function in disease risk or pathophysiology,

https://doi.org/10.1021/acsptsci.1c00233
ACS Pharmacol. Transl. Sci. 2022, 5, 156−168

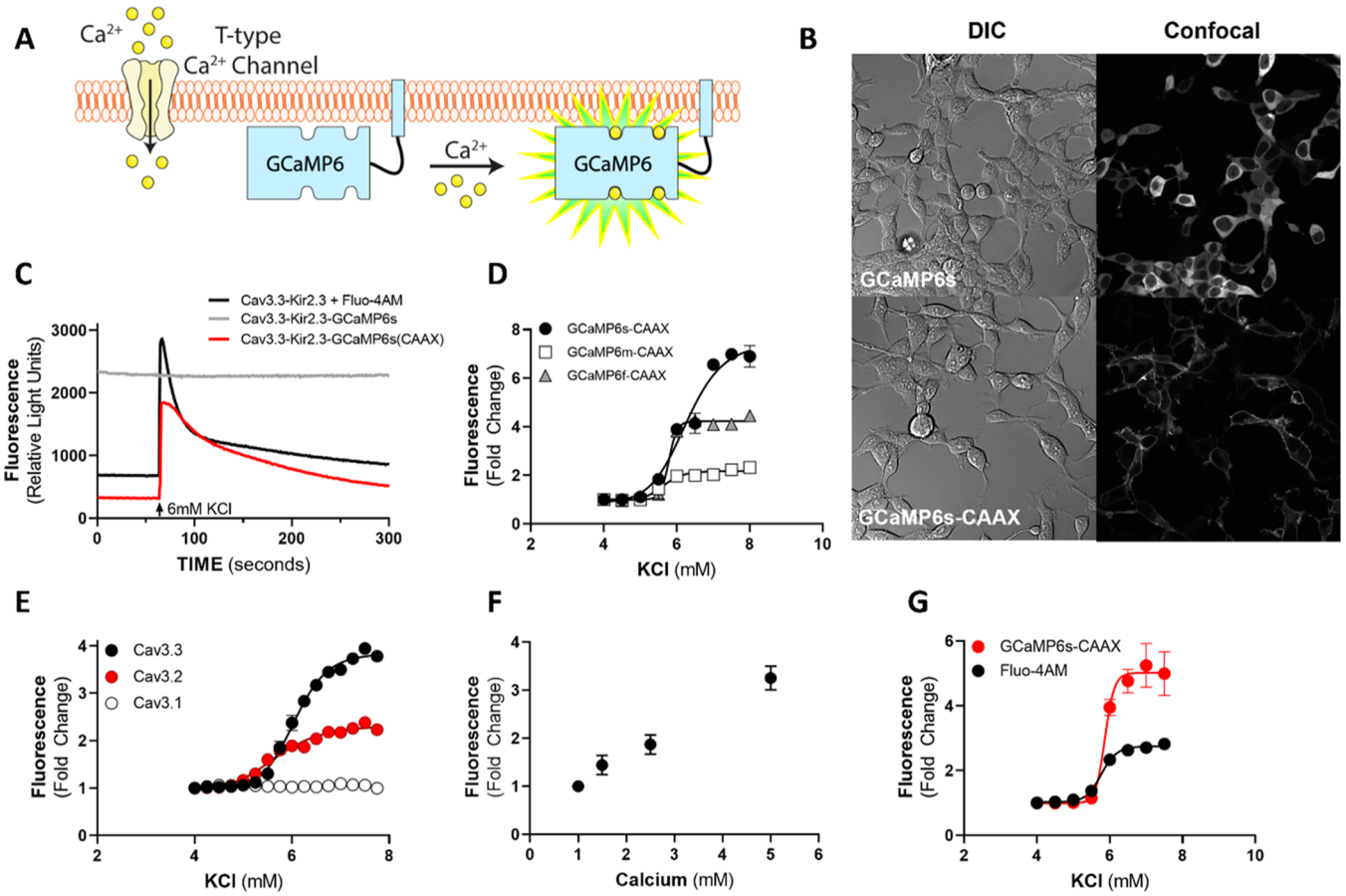

Figure 2. Development of a novel 384-well-based high-throughput assay to readout T-type Ca^{2+} channel activity using a membrane-tethered calcium sensor GCaMP6s-CAAX. (A) Schematic of GCaMP6s-CAAX in response to T-type Ca^{2+}-mediated Ca^{2+} influx. (B) Representative 60× images of HEK293 cells expressing $K_{ir}2.3/Ca_V3.3$ with GCaMP6s or GCaMP6s-CAAX. (Left) Differential interference contrast images. (Right) Fluorescence images demonstrating the cytosolic localization of GCaMP6s and the expression of GCaMP6s-CAAX near the plasma membrane. (C) FLIPR signal traces from the HEK293 cells expressing $Ca_V3.3/K_{ir}2.3$ in the presence of Fluo-4AM (black) or expressing either GCaMP6s (gray) or GCaMP6s-CAAX (red) when stimulated with 6 mM KCl. (D) KCl CRC of HEK293 cells expressing $K_{ir}2.3$ and $Ca_V3.3$ with GCaMP6s-CAAX (black), GCaMP6m-CAAX (gray), or GCaMP6f-CAAX (white) normalized to baseline fluorescence. (E) KCl CRC of HEK293 cells expressing $K_{ir}2.3$ and $Ca_V3.3$ (black), $Ca_V3.2$ (red), or $Ca_V3.1$ (white) normalized to baseline fluorescence. Data are expressed as mean ± SEM (24 replicates and 2 independent experiments). (F) FLIPR signal of HEK293 cells expressing $K_{ir}2.3$ and $Ca_V3.1$ with GCaMP6s-CAAX in response to a different Ca^{2+} concentrations (four replicates and two independent experiments). (G) KCl CRC in HEK293 cells expressing $K_{ir}2.3$ and $Ca_V3.3$ loaded with the Ca^{2+}-sensitive dye Fluo-4AM (black) or coexpressing GCaMP6s-CAAX (red). Data are expressed as mean ± SEM (24 replicates and 2 independent experiments).

and selective T-type Ca^{2+} channel potentiators may provide therapeutic benefit in certain disorders.

Due to the relatively distinct expression patterns of each T-type Ca channel[32] and because $Ca_V3.1$, $Ca_V3.2$, and $Ca_V3.3$ have been implicated in several distinct diseases,[2,18,21,22,25,30,33,34] the development of highly selective potentiators or inhibitors for each T-type Ca^{2+} channel may be beneficial. Activating or inhibiting all three T-type Ca^{2+} channels may induce unwanted side effects and could limit efficacy in human studies.

To date, multiple high-throughput Ca^{2+} influx assays using Ca^{2+} sensitive dyes have been developed to identify T-type Ca^{2+} channel inhibitors.[35−37] However, none addressed the critical need to identify T-type Ca^{2+} channel potentiators. While some assays used gramicidin treatment to control the membrane potential,[38] few T-type Ca^{2+} channel high-throughput screening (HTS) assays have been designed with physiological conditions relevant for neuronal cells (e.g., an intact resting membrane potential of −70 mV), and this has likely hampered the ability of these assays to identify T-type Ca^{2+} channel potentiators. Furthermore, while Ca^{2+} sensitive dyes have been the gold standard for HTS, the high cost of reagents and the time it takes to load the dye and subsequent multiple washing steps are major limitations of this technology.

To address these issues and develop an assay that can identify both inhibitors and potentiators, we developed inducible T-type Ca^{2+} channel cell lines expressing $K_{ir}2.3$, an inward rectifying potassium channel that can hyperpolarize HEK293 cells to −70 mV, thus creating a physiological membrane potential representative of neuronal cells where most T-type Ca^{2+} channels are available to open. Additionally, we developed a membrane-tethered version of the stable ultrasensitive Ca^{2+} sensor GCaMP6s (GCaMP6s-CAAX) that showed a significantly higher signal window than either the untethered GCaMP6 or the Ca^{2+} sensitive dye, Fluo-4AM. This GCaMP6s-CAAX assay performs well (R^2 = 0.768, p < 0.0001) in comparison to Fluo4-AM using a small screen of select known Ca^{2+} channel antagonists. Lastly, we utilized the membrane-tethered GCaMP6s-CAAX in multiple cellular assays measuring changes in the intracellular Ca^{2+} concen-

https://doi.org/10.1021/acsptsci.1c00233
ACS Pharmacol. Transl. Sci. 2022, 5, 156−168

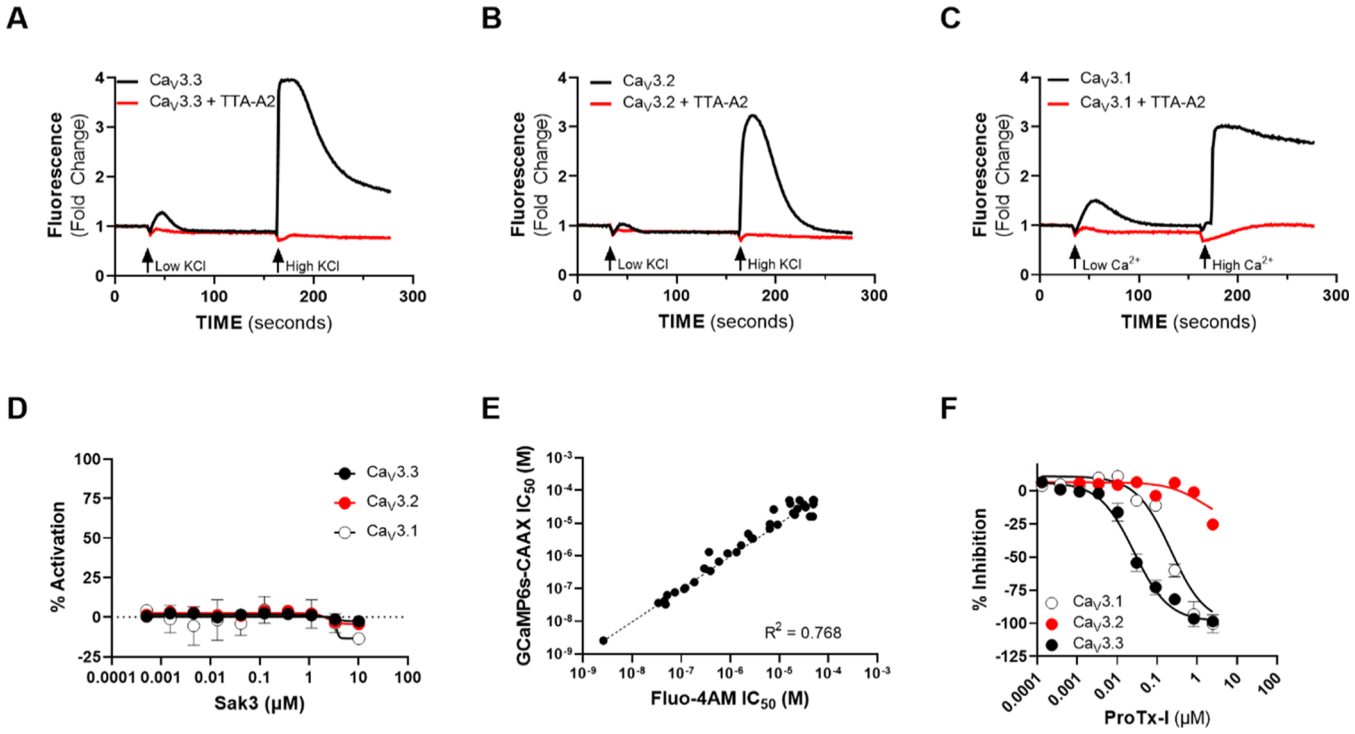

Figure 3. The novel GCaMP6s-CAAX assay can identify both activators and inhibitors of T-type Ca^{2+} channels. (A) Representative fluorescence sample traces of HEK293 cells expressing $Ca_V3.3/K_{ir}2.3$/GCaMP6s-CAAX in the presence of 5.4 mM (low) or 6.7 mM (high) KCl. (B) Sample traces of HEK293 cells expressing $Ca_V3.2/K_{ir}2.3$/GCaMP6s-CAAX in the presence of 4.7 mM (low) or 6.0 mM (high) KCl. (C) Sample trace of HEK293 cells expressing $Ca_V3.1/K_{ir}2.3$/GCaMP6s-CAAX in the presence of 1.5 mM (low) or 5.0 mM (high) $CaCl_2$. Cells were treated with DMSO (black) or 1 μM of the pan T-type Ca^{2+} channel inhibitor TTA-A2 (red). Traces were normalized to baseline prestimulation fluorescence. (D) CRC of SAK3 in HEK293 cells expressing $K_{ir}2.3$/GCaMP6s-CAAX with $Ca_V3.1$ (white), $Ca_V3.2$ (red), or $Ca_V3.3$ (black). Data are expressed as mean ± SEM of two independent experiments. (E) The IC_{50} values of 42 different compounds evaluated using GCaMP6s-CAAX are plotted against the IC_{50} values of the same compounds evaluated using the Ca^{2+}-sensitive dye Fluo-4AM. (F) ProTx-I CRC in cells expressing $Ca_V3.1$ (white), $Ca_V3.2$ (red), and $Ca_V3.3$ (black). Data are expressed as mean ± SEM of two independent experiments.

tration mediated by endogenous G-protein-coupled receptor (GPCR) activity, thereby demonstrating the flexibility and broad applicability of GCaMP6s-CAAX in a range of Ca^{2+} assays. We conclude that the GCaMP6s-CAAX fluorescent sensor offers a highly sensitive and flexible approach to establish high-throughput cell-based Ca^{2+} assays of endogenous and exogenous receptors.

RESULTS

Biophysical and Pharmacological Properties of T-Type Calcium Channels Stably Expressed in the Presence of $K_{ir}2.3$. We established an inducible expression system that stably integrates a single copy of cDNA encoding $Ca_V3.1$, $Ca_V3.2$, or $Ca_V3.3$ in HEK293 cells separately using the Flp-In T-REx system, as previously published.[30] The expression of each of the three human Ca_V3 channels was induced by 1 μg/mL doxycycline treatment as described previously[30] and confirmed via western blot (Supporting Information Figure S1). Using an automated planar patch-clamp instrument (SyncroPatch 384PE) that offers giga-ohm seal and precise voltage control, we characterized the electrophysiological properties of each of these three T-type Ca^{2+} channels using the protocol described previously[39] (Figure 1A). All three Ca_V3 channels displayed classic characteristics in kinetics (Figure 1B), voltage dependence of activation (Figure 1C), voltage dependence of inactivation (Figure 1D), and demonstrated similar peak current density (Figure 1E). It is worth noting that the inactivation kinetics of $Ca_V3.3$ is an order of magnitude lower compared to that of $Ca_V3.1$ and $Ca_V3.2$ and that $Ca_V3.3$ opens and inactivates at more positive potentials, revealing distinct biophysical properties for $Ca_V3.3$ that are consistent with existing reports.[10]

At the typical −25 mV resting membrane potential of HEK293 cells,[40] T-type Ca^{2+} channels are largely inactivated and cannot open to allow Ca^{2+} influx upon depolarization by KCl treatment.[41] We therefore stably expressed $K_{ir}2.3$ inward rectifier channels in these cells to shift the resting membrane potentials close to the predicted potassium equilibrium potential of −70 mV and remove the inactivation of T-type Ca^{2+} channels. The presence of $K_{ir}2.3$ channels hyperpolarized the membrane voltage to −70 mV at the typical 4 mM extracellular K^+ concentration, as measured by the whole-cell patch clamp (Figure 1F), and the increased extracellular K^+ concentrations depolarized the membrane potentials in a KCl concentration-dependent manner. Collectively, we established cell lines that recapitulate the physiological membrane potentials of neurons and allow for the high-throughput evaluation of compounds to identify modulators of T-type Ca^{2+} channel functions.

Development of the T-Type Calcium Channel Fluorescence Assay Using the Membrane-Tethered Genetic Calcium Sensor GCaMP6s-CAAX. Calmodulin-based genetically encoded fluorescent Ca^{2+} indicators (GCaMP-s) are powerful tools to image Ca^{2+} dynamics from cells in a plate to intact behaving animals. GCaMP6 indicators produce bright fluorescence induced by Ca^{2+} binding and have

https://doi.org/10.1021/acsptsci.1c00233
ACS Pharmacol. Transl. Sci. 2022, 5, 156−168

been widely used to measure cytosolic Ca^{2+} concentrations.[42] To reduce the background noise and to facilitate the measurement of T-type Ca^{2+} channel activity, we tagged the genetically encoded fluorescence sensor GCaMP6s with a CAAX box to the C-terminus to localize the sensor to the plasma membrane (Figure 2A). The CAAX box is composed of a cysteine residue (C), two aliphatic residues (AA), and any C-terminal amino acid (X), and this sequence can undergo prenylation, a process in which post-translational lipid additions occur, thereby creating a hydrophobic C-terminus and thus greatly increasing the ability of the protein to interact with the plasma membrane.[43,44] We then stably incorporated our membrane-tethered GCaMP6s-CAAX sensor into our $Ca_V3/K_{ir}2.3$ cell lines and demonstrated GCaMP6s-CAAX localization at the plasma membrane (Figure 2B). Using the high-throughput fluorometric imaging plate reader (FLIPR), the membrane-tethered GCaMP6s-CAAX resulted in a dramatically reduced baseline signal before stimulation compared to the untethered GCaMP6s and the calcium-sensitive dye Fluo-4AM (Figure 2C).

There exist multiple variants of GCamp6, with distinct kinetic properties. Therefore, we evaluated which of the three previously described variants of GCaMP6: GCaMP6 slow, GCaMP6 medium, and GCaMP6 fast (GCaMP6s, GCaMP6m, and GCaMP6f, respectively[42]), produce the largest fluorescence signal in cells expressing $Ca_V3.3$ channels upon KCl stimulation. In agreement with previously described GCaMP6 variant findings,[42] we found that GCaMP6s produced a much larger T-type Ca^{2+} channel signal window induced by KCl depolarization compared to GCaMP6m or GCaMP6f (Figure 2D). Importantly, KCl stimulation-induced increase in fluorescence was absent in cells without doxycycline-induced T-type Ca^{2+} channel expression (Supporting Information Figure S2). While GCaMP6s-CAAX produced a robust KCl stimulation-induced increase in fluorescence in both $Ca_V3.3$ and $Ca_V3.2$ cell lines, the $Ca_V3.1$-expressing cells had minimal KCl-induced responses (Figure 2E). To overcome the low response of GCaMP6s-CAAX to KCl in the $Ca_V3.1$-expressing cell line, we took advantage of the $Ca_V3.1$ window current by increasing the extracellular Ca^{2+} concentration to produce a reliable $CaCl_2$-dependent response in our $Ca_V3.1/K_{ir}2.3$-expressing cells (Figure 2F).

Having identified GCaMP6s-CAAX as our optimal genetically encoded Ca^{2+} sensor, we then directly compared the performance of GCaMP6s-CAAX to the Ca^{2+}-sensitive dye Fluo-4AM. Using the $Ca_V3.3$-expressing cells, GCaMP6s-CAAX produced a much larger signal window in response to KCl stimulation compared to Fluo-4AM (Figure 2G). Together, these results demonstrate that the membrane-tethered GCaMP6s-CAAX substantially improves the assay performance relative to Fluo-4AM, the field-standard synthetic Ca^{2+} sensitive dye.

Establishment of a Cell-Based HTS Assay That Can Identify Both Inhibitors and Potentiators of T-Type Calcium Channels. While many T-type Ca^{2+} channel inhibitors have been discovered, there are few known subtype selective antagonists[24] and no known subtype specific potentiators.[45,46] Therefore, using our $Ca_V3/K_{ir}2.3$/GCaMP6s-CAAX cell lines, we developed a cellular assay to identify both positive (potentiators) and negative (inhibitors) modulators of T-type Ca^{2+} channels. We implemented two KCl depolarization steps, separated by 3 min, to produce (1) an EC_{10} response for identifying potentiators and (2) a larger EC_{90} response for identifying inhibitors. For $Ca_V3.3$, 5.4 mM KCl addition produced an EC_{10} response and 6.7 mM KCl produced an EC_{90} response. Using this paradigm, we showed that the fluorescence signal was $Ca_V3.3$-dependent as the signal was blocked by the T-type Ca^{2+} channel inhibitor TTA-A2 (Figure 3A).

Similarly, we established $Ca_V3.2$ and $Ca_V3.1$ FLIPR assays following a similar protocol by coexpressing $K_{ir}2.3$ and GCaMP6s-CAAX with $Ca_V3.2$ or $Ca_V3.1$ in HEK293 cells. We titrated the concentrations of KCl to induce $Ca_V3.2$-mediated Ca^{2+} influx and found that 4.7 and 6.0 mM KCl corresponds to a $Ca_V3.2$ EC_{10} and EC_{90} response, respectively (Figure 3B). While $Ca_V3.1$-expressing cells do not respond well to KCl-induced depolarization alone (Figure 2E), $Ca_V3.1$-mediated Ca^{2+} influx through window currents increased with extracellular Ca^{2+} concentration. We were then able to optimize Ca^{2+} flux in the presence of 1.5 and 5 mM $CaCl_2$, respectively, for identifying $Ca_V3.1$ potentiators and inhibitors (Figure 3C). Using the high KCl or high Ca^{2+} concentration as the positive control across the plates, Z' calculations in the activator mode for all three T-type Ca^{2+} channel assays were 0.7, 0.5, and 0.3 for $Ca_V3.3$, 3.2, and 3.1, respectively, indicating assay performance suitable for HTS.

Recently, SAK3 was reported to enhance the Ca_V3 function in neurons,[47−49] but its binding or direct effect on Ca_V3 channels is yet to be established. Therefore, we evaluated both SAK3 and the previously disclosed nonselective T-type Ca^{2+} channel potentiator ST-101 in our GCaMP6s/Kir2.3/Cav3 cell lines. Unfortunately, neither SAK3 (Figure 3D) nor ST-101 (Supporting Information Figure S3) displayed potentiator activity in any of the three T-type Ca^{2+} channel cell-based assays. Due to the absence of established potentiators of T-type Ca^{2+} channel activity, we were not able to validate the assay for this modality using chemical compounds. However, by using a library of more than 40 channel modulators[2,27,34,50] (Table 1), we demonstrated that the IC_{50} values of the GCaMP6s-CAAX-based assay significantly correlated (R^2 = 0.768, $p < 0.0001$) with the IC_{50} values of the Fluo-4AM-based assay (Figure 3E), confirming that the GCaMP6s-CAAX-based FLIPR assay produces similar results to those previously published.[34] Utilizing this validated assay, we then evaluated the subtype-specific Ca_V3 channel activity of the previously described T-type Ca^{2+} channel inhibitor ProTx-I[51,52] in all three cell lines. Interestingly, we found that ProTx-I displays potent antagonist activity at $Ca_V3.3$ (IC_{50} = 0.026 μM) with reduced potency toward $Ca_V3.1$ (IC_{50} = 0.22 μM) and greatly reduced activity at $Ca_V3.2$ (IC_{50} = 1.4 μM) (Figure 3F). Taken together, we developed high-throughput GCaMP6s-CAAX-based FLIPR assays across the three Ca_V3 channels that can identify both inhibitors and potentiators.

Membrane-Tethered GCaMP6s-CAAX Has Broad Utility in Measuring Endogenous Receptor-Mediated Ca^{2+} Signaling. Since GCaMP6s-CAAX displays a superior signal window compared to the traditional Ca^{2+}-sensitive dyes in our T-type Ca^{2+} channel cell-based assays, we then tested the utility of GCAMP6s-CAAX in measuring Ca^{2+} signals originating from endogenous G-protein-coupled receptor activation—an application that may be useful to a broader scientific community. Previous studies have demonstrated that Chinese hamster ovary K1 cells (CHOK1) endogenously express the lysophosphatidic acid (LPA) 1 receptor subtype (LPA_1),[53] a member of the GPCR superfamily.[54] To measure endogenous LPA receptor activity, we expressed the

https://doi.org/10.1021/acsptsci.1c00233
ACS Pharmacol. Transl. Sci. 2022, 5, 156−168

Table 1. IC_{50} Values against $Ca_V3.3$ Obtained for the Selected Ion Channel Modulators Using the Novel FLIPR Assay

compound name	IC_{50} (μM)
tta-i1	0.0026
mk-8998	0.037
tta-a2	0.053
tta-p2	0.033
z-944	0.11
ml 218	0.077
penufluridol	0.097
tta-q4 (racemic)	0.16
NNC 55-0396 dihydrochloride	0.34
lercanidipine hydrochloride	0.41
mibefradil dihydrochloride	0.67
flunarizine dihydrochloride	1.2
lomerizine hydrochloride	1.3
nicardipine hydrochloride	2.1
loperamide hydrochloride	1.3
retigabine	9.4
benidipine hydrochloride	3.4
flupirtine maleate	3.5
sr 33805 oxalate	4.7
azelnidipine	26
carboxyamidotriazol orotate	6.8
felodipine	27
(*s*)-(−)-bay-k-8644	16
celecoxib	9.0
fpl 64176	31
ns1643	39
riluzole	50
nitrendipine	18
pd-173212	50
(*R*)-(+)-bay k8644	16
ns-3623	37
aconitine	50
gv-58	20
eszopiclone	50
amitriptyline hydrochloride	50
nefiracetam	50
amiloride hydrochloride	50
ascorbic acid	50
isradipine	38
zset 1446	50
ml297	50
Ica27243	50

GCaMP6s-CAAX sensor in the CHOK1-α15 cell line that expresses the promiscuous G-protein $G\alpha_{15}$. In this stable cell line, we demonstrate that lysoPA18:1 application generated a robust increase in the fluorescence signal that was blocked by the selective LPA_1 receptor antagonist AM095[55] (Figure 4A). Using this assay, we found that the application of the LPA_1 receptor agonist lysoPA18:1 resulted in a concentration-dependent increase in fluorescence (Figure 4B) with an EC_{50} of 1.01 ± 0.19 μM. Conversely, AM095 blocked the LPA_1-mediated signal in a concentration-dependent manner with an IC_{50} value of 0.24 ± 0.02 μM (Figure 4C). These data are consistent with the reported effects of these compounds on LPA_1 receptors,[55] validating our approach of using GCaMP6s-CAAX to measure GPCR activities.

The CHOK1 cells also endogenously express the complement C3a receptor, a GPCR that canonically signals through $G_{\alpha i}$.[56] Using the same CHOK1 cells expressing the GCaMP6s-CAAX sensor and the promiscuous G-protein $G\alpha_{15}$, we found that application of the 9 kD peptide human C3a (hC3a) resulted in a concentration-dependent increase in fluorescence (Figure 4D,E) with an EC_{50} of 4.5 ± 0.5 nM. Congruent with the previous literature,[57] hC3a treatment-induced increases in GCaMP6s-CAAX-mediated fluorescence were blocked by the C3a receptor antagonist BR111 in a concentration-dependent manner (Figure 4D,F), with an IC_{50} value of 2.5 ± 0.2 nM. Taken together, these studies demonstrate that the GCaMP6s-CAAX fluorescence sensor can be used to measure the effects of a wide range of endogenous GPCRs, expanding its utility in measuring the activities of a variety of endogenous and exogenous membrane receptors in cellular assays.

DISCUSSION

In the present studies, we developed cell lines that express the membrane-tethered genetically encoded Ca^{2+} sensor GCAMP6s-CAAX and demonstrated that GCaMP6s-CAAX displays a superior signal window over traditional Ca^{2+}-sensitive dyes such as Fluo-4AM. Our assay using the GCAMP6s-CAAX fluorescence sensor has the advantage of shorter assay time and lower assay costs compared to synthetic Ca^{2+} dyes by removing the need to load and subsequently wash off the fluorescent dye through multiple steps. Importantly, this membrane-tethered Ca^{2+} sensor performed much better than GCaMP6s alone in HEK293 cells (Figure 2C), underscored by a much-reduced baseline fluorescence signal prior to stimulation. The high level of background fluorescence when using GCaMP6s may be due to a small but significant constitutive Ca^{2+} window current that raised the cytosolic background of Ca^{2+}[58] as T-type Ca^{2+} channels are expressed in these cells. In evaluating over 40 distinct T-type Ca^{2+} channel inhibitors, we demonstrated that HEK293 cells expressing both GCaMP6s-CAAX and $K_{ir}2.3$ produced similar results as the gold-standard Ca^{2+}-sensitive dye, Fluo-4AM. While genetically encoded sensors can be readily packaged into viral vectors for delivery and usage with wide applications,[42,59] it is important to note that they require exogenous expression, a potential disadvantage over dyes such as Fluo-4AM. Furthermore, we used our high-throughput T-type Ca^{2+} channel assay to characterize the subtype selectivity of the T-type Ca^{2+} channel antagonist ProTx-1. Lastly, we demonstrated that GCaMP6s-CAAX can be used to measure the receptor activity of two distinct GPCRs endogenously expressed on CHOK1 cells, thereby demonstrating the potential use of GCaMP6s-CAAX in a wide range of biological applications including neuroscience, cancer, infectious diseases, and other areas of drug discovery interest.

While genetic models have revealed certain specific neurobiological functions of each of the three T-type Ca^{2+} channels,[29,31,33,60−62] developmental or cellular compensatory mechanisms in a genetic model may confound the findings. Therefore, subtype-selective T-type Ca^{2+} channel modulators would be powerful pharmacological tools to study subtype-specific T-type Ca^{2+} channel biology. Furthermore, while current efforts focus on T-type Ca^{2+} channel inhibitors being potentially beneficial for diseases such as epilepsy, pain, and certain cancers,[2,24,34] recent human genetic studies have also identified loss of function of $Ca_V3.1$ and $Ca_V3.3$ in neuropsychiatric disease risk.[29,30,63] Therefore, specific T-type Ca^{2+}

https://doi.org/10.1021/acsptsci.1c00233
ACS Pharmacol. Transl. Sci. 2022, 5, 156−168

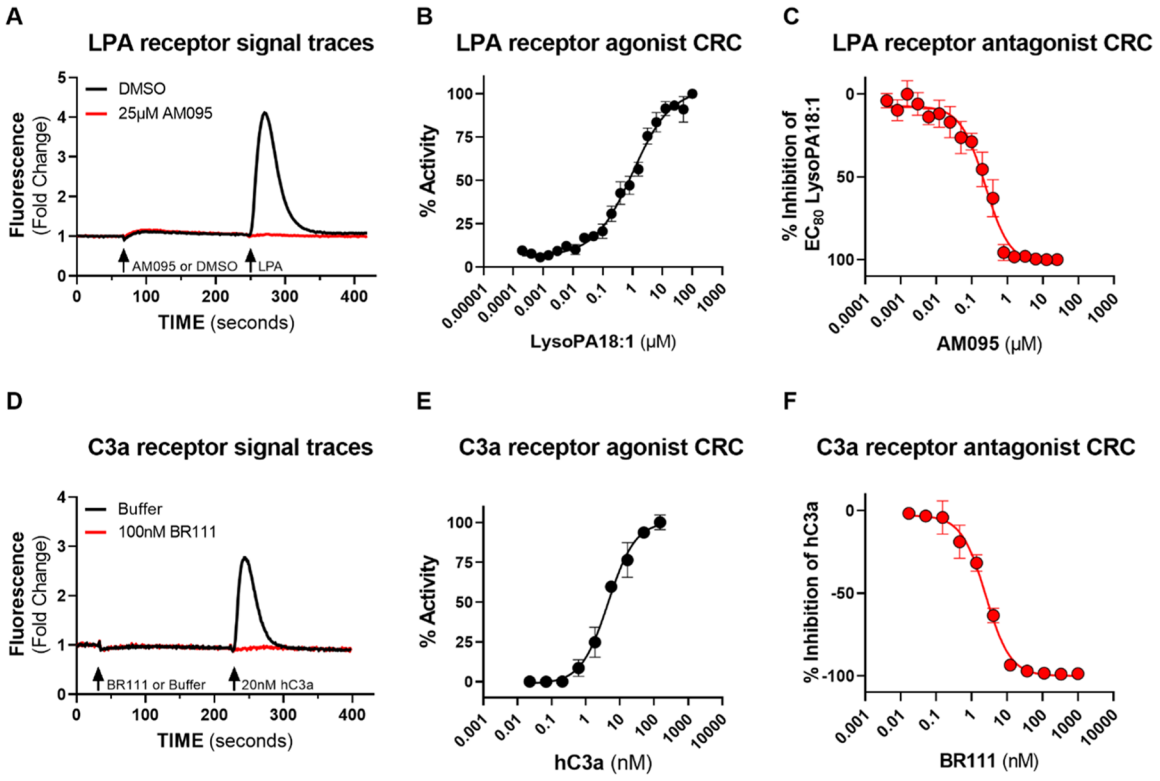

Figure 4. Assays utilizing GCAMP6s-CAAX can be used to effectively evaluate the endogenous activity of GPCRs. (A) Representative sample traces of endogenous LPA_1 receptor activity in CHOK1 cells expressing GCaMP6s-CAAX and $G\alpha_{15}$ in the presence of DMSO (black) or 25 μM AM095 (red) normalized to baseline prestimulation fluorescence. (B) CRC of lysoPA18:1 induced endogenous LPA_1 receptor activity in CHOK1 cells expressing GCaMP6s-CAAX and $G\alpha_{15}$. (C) CRC of the selective LPA_1 receptor antagonist AM095 in CHOK1 cells expressing GCaMP6s-CAAX and $G\alpha_{15}$. (D) Representative sample traces of endogenous C3a receptor activity in CHOK1 cells expressing GCaMP6s-CAAX and $G\alpha_{15}$ in the presence of a buffer (black) or 100 nM BR111 (red) normalized to baseline prestimulation fluorescence. (E) CRC of hC3a induced endogenous C3a receptor activity in CHOK1 cells expressing GCaMP6s-CAAX and $G\alpha_{15}$. (F) CRC of the C3a receptor antagonist BR111 in the presence of 20 nM hC3a in CHOK1 cells expressing GCaMP6s-CAAX and $G\alpha_{15}$. Data are expressed as mean ± SEM of four replicates from two independent experiments.

potentiators may provide therapeutic benefit in diseases in which the goal is to enhance T-type Ca^{2+} channel functions.

Recently, SAK3 was reported to enhance Ca_V3 functions and improve cognitive performance in a number of animal models.[47−49] However, we found that SAK3 did not stimulate any Ca_V3 channels directly in our FLIPR assays (Figure 3D) when applied in a similar method as previously described[46] and therefore believe that SAK3 works indirectly through other targets. In this study, we did not set out to screen nor did we identify any T-type Ca^{2+} channel activators. However, our GCAMP6s-CAAX high-throughput assay can identify both inhibitors and potentiators and, in conjunction with compound screening libraries enriched with favorable drug-like properties (e.g., high brain permeability, low CYP450 activity, and high solubility),[64,65] could produce tractable drug discovery chemical matter hits with relatively low cost compared to traditional HTS. It is important to note that the $Ca_V3.1$ assay does not respond to KCl depolarization as well as $Ca_V3.3$ or $Ca_V3.2$ assays (Figure 1E). We currently do not know what accounts for the inability of $Ca_V3.1$ to respond to KCl as the whole-cell current density is similar across all three Ca_V3 cell lines (Figure 1B,E). However, $Ca_V3.1$ responds well to the changes in extracellular Ca^{2+} (Figure 2F), and therefore, we are confident that $Ca_V3.1$ activity can be evaluated using changes in Ca^{2+} levels in place of changes in KCl concentrations. Therefore, this assay is amenable for both the pharmaceutical industry and academic research centers.

Interestingly, ProTx-I has been previously characterized as a potent $Ca_V3.1$ antagonist with 10-fold selectivity over $Ca_V3.3$ and 100-fold selectivity over $Ca_V3.2$.[51,52] This contrasts our findings in which ProTx-I displays potent $Ca_V3.3$ antagonist activity with relatively lower antagonist activity at $Ca_V3.1$ and the lowest antagonist activity at $Ca_V3.2$ (Figure 3F). These differences in ProTx-I selectivity may be due to a number of reasons including the fact that we utilized our high-throughput FLIPR assay to perform a full concentration response curve (CRC) in all three T-type Ca^{2+} channel cell lines, whereas previous reports only evaluated ProTx-I at one concentration.[51,52] Furthermore, previous reports have shown that certain T-type Ca^{2+} inhibitors, such as TTA-A2, can display state dependence and preferentially interact with T-type Ca^{2+} channels in the inactivated state.[66] Therefore, the differences in the holding potential between our Cav3/Kir2.3/GCaMP62-CAAX cell lines (−70 mV) and what was previously published using ProTx-I (−110 mV)[52] may also account for the difference in findings. While we were able to replicate the previous findings that ProTx-I displays the weakest antagonist activity at $Ca_V3.2$ compared to other T-type Ca^{2+} channels, detailed biophysical characterization of this toxin using patch clamp electrophysiology will be necessary to resolve these conflicting results.

https://doi.org/10.1021/acsptsci.1c00233
ACS Pharmacol. Transl. Sci. 2022, 5, 156−168

To date, synthetic and genetically encoded Ca^{2+} sensors have been well established for measuring cellular Ca^{2+} dynamics mediated by both ion channels[37] and GPCRs.[67] Here, we extended the application of a membrane-tethered GCAMP6-CAAX to measure endogenous GPCR activities (Figure 4). While we did not directly compare the signal-to-background ratio between GCAMP6s-CAAX and GCAMP6s in the GPCR assays, our application of the membrane-tethered GCAMP6-CAAX displayed excellent performance in measuring GPCR activities with a maximum receptor activity signal/noise ratio of 3−4, which is similar to our T-type Ca^{2+} channel findings. Also, akin to the T-type Ca^{2+} channel GCaMP6s-CAAX assay, the GPCR GCaMP6s-CAAX assay allows for the simultaneous identification of both inhibitors and activators in one experiment using two agonist additions. Compounds that act as inhibitors or potentiators in the FLIPR assay can then be confirmed using in vitro electrophysiology and counter-screened using a thallium flux assay to measure $K_{ir}2.3$ activity as described previously.[68] Overall, we demonstrate that the GCAMP6s-CAAX assay format is both versatile and informative.

Lastly, as newer genetically encoded sensors continue to be developed for Ca^{2+}[59] and other key signaling pathways such as cAMP,[69] it will be important to test whether membrane-tethered forms of these sensors are better suited for HTS efforts than their cytosolic counterparts. Plasma membrane-tethered genetically encoded sensors are beneficial for channels and receptors located at the plasma membrane but would not be effective for signaling localized to subcellular compartments. Previously, genetically encoded sensors for specific subcellular organelles (e.g., endoplasmic reticulum, endosomes, lysosomes, mitochondria, etc.) have been described;[70−72] however, few of these sensors have been evaluated for use in HTS. Thus, through the detailed characterization of the capability of using these subcellular specific genetically encoded sensors in HTS assays, in addition to plasma membrane-tethered sensors such as GCaMP6s-CAAX, researchers would have a diverse toolbox of localized sensors that can be readily applied to translational drug discovery efforts.

METHODS

Molecular Biology and Compounds. The cDNA sequences of $Ca_V3.1$ (NM_018896.3), $Ca_V3.2$ (NM_021098.2), and $Ca_V3.3$ (NM_021096) were subcloned into a modified pFRT-TO vector with an in-frame C-terminal FLAG tag, as previously described. pCMV-GCaMP6, pCMV-GCaMP6s-CAAX, pCMV-GCaMP6m, and pCMV-GCaMP6f were obtained from Addgene (40753, 52228, 40754, and 40755, respectively). The PmlI-NotI C-terminal fragment of pCMV-GCaMP6s-CAAX was subcloned into pCMV-GCaMP6m and pCMV-GCaMP6f to generate pCMV-GCaMP6m-CAAX and pCMV-GCaMP6f-CAAX. The P2A-puroR sequence of pLenti-A2D1-P2A-puroR (Origene RC219081) was PCR-amplified with oligos containing MluI and PmeI cut sites and subcloned into pLenti-KCNJ4-GFP (Origene RC222272L2) to generate pLenti-KCNJ4-P2A-puroR.

Compounds Used. ML297 and AM095 were purchased from Sigma-Aldrich (St. Louis, MO). (*S*)-(−)-BAY-K-8644, (*R*)-(−)-BAY-K-8644, and SAK3 were obtained from Tocris Bioscience (Bristol, UK). lysoPA18:1 was purchased from Avanti Polar Lipids Inc. (Alabaster, AL). hC3a was purchased from Complement Technology Inc. (Tyler, TX). Fluo-4AM was purchased from Thermo Fisher Scientific Inc. (Waltham, MA). MK-8998, ST101, TTA-I1, and TTA-A2 were synthesized in house. All other compounds were obtained from Alomone Labs (Jerusalem, Israel).

Construction of Stable Single-Copy-Inducible FlpIn TREx 293 Cell Lines Constitutively Expressing Both the Inward Rectifying K^+ Channel KCNJ4 and Membrane-Tethered Genetic Calcium Sensors. Inducible FlpIn TREx cell lines that express a single isogenic copy of $Ca_V3.1$, $Ca_V3.2$, or $Ca_V3.3$ cDNA were generated and validated as previously described.[30] 3 μg of pLenti-KCNJ4-P2A-puroR was transfected with Lipofectamine 2000 at a 1:2 ratio in Optimem into these cell lines and selected with 1.25 μg/mL of puromycin to generate a polyclonal line for each Ca_V3 channel. Next, 3 μg of CMV-GCaMP6s/m/f with a C-terminal CAAX motif (from Addgene) was transfected as above into these cell lines and selected with 300 μg/mL of neomycin. Clonal lines were selected under a fluorescent picking scope for proper membrane localization and expanded before testing. The cells were passaged once in media containing 300 μg/mL neomycin and then maintained in media containing 1.25 μg/mL puromycin for less than 30 passages. Antibiotics were absent in the cell media for all the assay plates.

Construction of Stable CHOK1 Cell Lines Constitutively Expressing Both $G\alpha_{15}$ and Membrane-Tethered Genetic Calcium Sensors. CHOK1-α15 was purchased from Genscript and maintained in the F-12K medium (ATCC 30-2004) + 10% fetal bovine serum (FBS). The GCaMP6s-CAAX construct was purchased from Addgene. 3 μg of CMV-GCaMP6s-CAAX motif was transfected into CHOK1-α15 cell lines with Lipofectamine 2000 at a 1:2 ratio in Optimem and selected with 700 μg/mL G-418. The clonal lines were selected under a fluorescent picking scope based on GCaMP basal green fluorescence and ATP-stimulated GCaMP fluorescence change in the CHOK1 clone.

FLIPR Assay for T-Type Calcium Channels Using GcaMP6s-CAAX. The cells were maintained in DMEM/F-12 + GlutaMAX + 10% FBS + 1.25 μg/mL puromycin. Two days prior to conducting the assay, the $Ca_V3/K_{ir}2.3$/GCaMP6 cells were seeded at 16k/well density in the presence of 1 μg/mL doxycycline into poly-D-lysine-coated 384-well clear-bottom plates using a Multidrop Combi dispenser (Thermal Fisher). The cell plates were incubated in a 5% CO_2 humidified incubator at 37 °C for 2 days. On the day of the assay, the medium was aspirated using a plate washer, and 25 μL of the equilibrium buffer was added to each well. The assay plates were incubated for ∼60 min at room temperature in the dark and then placed in the FLIPR^{TETRA} instrument (Molecular Devices). Changes in fluorescence were measured over time with an excitation at 470−495 nm and an emission at 515−575 nm using a "two-addition" stimulation protocol measured at a 1 Hz sampling rate. After 30 s of baseline reading, 25 μL of the first stimulation, buffer 1, containing the EC_{10} concentration of KCl in the equilibrium buffer was added for the evaluation of agonist activity. The fluorescence emission was recorded for additional 120 s. To evaluate antagonist activity, 25 μL of the second stimulation, buffer 2, containing the EC_{90} concentration of KCl in the equilibrium buffer was added and recorded for another 120 s. The equilibrium buffer contained 133 mM NaCl, 10 mM HEPES, 10 mM D-glucose, 4 mM KCl, and 1 mM $CaCl_2$ and was adjusted to pH 7.3 using NaOH. The assay was performed at room temperature. The peak response over baseline from FLIPR^{TETRA} after each KCl

https://doi.org/10.1021/acsptsci.1c00233
ACS Pharmacol. Transl. Sci. 2022, 5, 156−168

addition was used for data analysis. KCL was used to induce T-type Ca^{2+} channel activity. For agonist evaluation, KCl was used to induce T-type Ca^{2+} channel activity and the minimum agonist response (0%) was the fluorescence response to the low KCl (EC_{10}) stimulation, and the maximal agonist response (100%) was the fluorescence response to a saturating concentration of 7 mM KCl. For antagonist evaluation, the maximal inhibition response (−100%) was the fluorescence response to the EC_{90} KCL stimulation in the presence of TTA-A2 (T-type Ca^{2+} channel inhibitor) at a saturated concentration (10 μM).The minimal inhibition (0%) was the fluorescence response to the EC_{90} KCl stimulation in the absence of TTA-A2.

FLIPR Assays for Endogenous GPCRs Using GCaMP6s-CAAX. The evaluation of GCaMP6s-CAAX to measure endogenous LPA_1 and C3a receptor activity was performed similar to the T-type Ca^{2+} channel GCaMP6s-CAAX assay. The CHOK1-α15 cells with the stable expression of GCaMP6s-CAAX were maintained in the F-12K medium (ATCC 30-2004) + 10% FBS + hygromycin (100 μg/mL) and G-418 (700 μg/mL). Two days prior to conducting the assay, the CHOK1/$G_{\alpha 15}$/GCaMP6s-CAAX cells were seeded at 16k/well density in 384-well clear-bottom plates using a Multidrop Combi dispenser. The cell plates were incubated in a 5% CO_2 humidified incubator at 37 °C for 2 days. On the day of the assay, the medium was aspirated using a plate washer and 25 μL of the equilibrium buffer was added to each well. The assay plates were incubated for 30 min at 37 °C in the dark and then placed in the $FLIPR^{TETRA}$ instrument (Molecular Devices). The assay was performed at 37 °C. Changes in fluorescence were measured over time with an excitation at 470−495 nm and an emission at 515−575 nm using a "two-addition" protocol measured at a 1 Hz sampling rate. In the first addition, compounds of interest were added for the evaluation of their agonist activity. In the second addition, an EC_{80} concentration of the corresponding agonist of the respective receptor was added in the presence of the experimental compound for the evaluation of antagonist activity. The assay buffer contained Hank's balanced salt solution with 20 mM HEPES and 0.1% BSA (fat acid-free Sigma A8806) at pH 7.3. The peak response over baseline from $FLIPR^{TETRA}$ after each addition was used for data analysis. For agonist evaluation, the minimum agonist response (0%) was the fluorescence response to buffer, and the maximum agonist response (100%) was the fluorescence response to the agonist at a saturated concentration. For antagonist evaluation, the maximal inhibition response (−100%) was the fluorescence response to the EC_{80} agonist stimulation in the presence of the GPCR inhibitor at a saturated concentration. The minimal inhibition (0%) was the fluorescence response to a EC_{80} agonist stimulation in the absence of the GPCR antagonist.

Western Blotting. Whole cell lysates of Flp-In T-REx HEK293 cells expressing Ca_V3 channels were prepared as previously described.[30] Electrophoresis samples were prepared in 4× Laemmli buffer (Bio-Rad) and incubated at room temperature for 20 min before SDS-PAGE (3−8% tris-acetate gel, Life Technologies). Antibodies: mouse anti-FLAG (1:1000, Sigma F1804), mouse anti-β-actin (1:50,000, Sigma A5441), mouse anti-β-tubulin (1:500, Cell Signaling Technology 86298S), and rabbit anti-$Ca_V3.1$ (1:500, Alomone Labs ACC-021). Anti-β-actin or β-tubulin signals were used as reference signals to normalize across preparations and to act as gel-loading controls.

Automated Patch-Clamp Electrophysiology. Automated patch-clamp electrophysiology experiments were performed using the SyncroPatch 384PE platform (Nanion Technologies) that can record up to 384 independent cells simultaneously with giga-ohm resistance seals. Recording solutions and experimental pipelines have been described previously.[39,73] In brief, for Ca^{2+} channel recordings, the cells were harvested 72 h after the induction of 1 μL/mL doxycycline. The cells were harvested, pelleted, and resuspended in serum-free DMEM F12-GlutaMAX (Thermo Fisher Scientific) and physiological extracellular solution (pECS) 50% (v/v). After resuspension, the cells were kept until the moment of the experiment in a temperature-controlled dedicated reservoir at 10 °C and shaken at 200 rpm. The experiments were performed within 1 h after the harvesting process. The assays were carried out in single-hole chips with resistances between 4 and 5 MΩ with the following solution (in mM): pECS 10 HEPES, 140 NaCl, 5 glucose, 4 KCl, 2 $CaCl_2$, 1 $MgCl_2$, 295−305 mOsm, pH 7.4 adjusted using NaOH. Internal recording solution (in mM): 20 EGTA, 10 HEPES, 50 CsCl, 10 NaCl, 60 CsF, 285 mOsm, pH adjusted to pH 7.2 by 1 N CsOH. The recording procedure and data analyses have been previously described.[39] The junction potential (∼12 mV) and the fast capacitive component were compensated; then, 15 μL of the cell suspension (50% v/v pECS/DMEM no serum) was added to each well to a final density of 50−80k cells/mL. All recording solutions were prepared with ultrapure MilliQ water (18 MΩ cm) and filtered with a 0.22 μm PES membrane and stored at 4 °C until use. The whole-cell configuration was achieved by a brief negative pressure pulse of −200 mbar. The holding potential was set at −100 mV for all the voltage protocols. Once in the whole-cell configuration, the slow capacitive component (C_{slow}) was canceled, and the series resistance (R_s) compensation was set at 80%. The data were acquired at 20 kHz and filtered at 10 kHz using Nanion proprietary software PatchControl 384 software (v.1.4.5). The data was processed on DataControl384 version 1.5.0 in real time using the quality checkpoints along the experiment using seal resistance, capacitance, and series resistance as qualitative parameters. The peak current and the activation steady-state parameters were obtained from currents elicited by a two-pulse protocol. The voltage-dependent activation and voltage-dependent inactivation protocols have been previously described.[39] The cells were initially held at −100 mV for 100 ms and then held for 1 s at a range of voltages from −120 to 20 mV with a 10 mV increase per sweep (TP1), followed by a 200 ms test pulse at −20 mV (TP2), concluding with 50 ms at −100 mV before the next step. The peak current density value was calculated as the maximum peak current from the preconditioning pulse normalized by the capacitance. The normalized chord conductance (G/G_{max}) was calculated from the $I-V$ relationship constructed with the peak current values for each voltage during TP1 using the following equation

$$G(V) = \frac{I_{peak}(V)}{(V - V_{rev})}$$

where V_{rev} is the reversal potential obtained using a linear extrapolation of the last four points of the $I-V$ relationship mentioned above. The voltage activation process was fitted using a single Boltzmann function

https://doi.org/10.1021/acsptsci.1c00233
ACS Pharmacol. Transl. Sci. 2022, 5, 156−168

$$G(V) = \frac{G_{max}}{1 + e^{-z\delta F(V - V_h)/RT}}$$

G_{max} is defined as the maximum value of G when the first derivative of G is minimal, $z\delta$ corresponds to the slope of the function and represents the voltage dependency of the activation, and V_h is the voltage at which half of the G_{max} is obtained. R corresponds to the universal gas constant, T is the absolute temperature in kelvin, and F is the Faraday constant. The steady-state inactivation parameters were obtained from the peak current values during TP2, which represent the fraction of channels able to be opened at the end of TP1. The voltage inactivation was also fitted using a single Boltzmann function to estimate.

Manual Patch-Clamp Electrophysiology. Whole-cell manual patch-clamp electrophysiology recordings were performed as previously described.[30] In brief, the recording solution contained 2 mM $CaCl_2$, 10 mM HEPES, and 140 mM NaCl, with the pH adjusted to 7.2 with NaOH. Pipettes were filled with an internal solution containing 126 mM CsCl, 10 mM EGTA, 1 mM EDTA, 10 mM HEPES, and 4 mM MgATP, with pH 7.2 adjusted with CsOH. The membrane potentials were recorded in the current clamp mode and clamped at 0 pA. An Axopatch 200B amplifier (Molecular Devices, LLC) was used for sampling at 20 kHz and filtered at 2 kHz. Each cell was then exposed to the recording solution containing increasing concentrations of KCl from 4.0 to 10.0 mM. All recordings were obtained at room temperature.

Ca^{2+}-Dependent Fluorescence Measurements. *Microscope Image Acquisition.* 50k cells were plated on 35 mm glass bottom dishes (Mat-Tek) with or without 1 μg/mL doxycycline for 48 h. The cells were incubated in the assay buffer (133 mM NaCl, 10 mM HEPES pH 7.4, 10 mM glucose, 4 mM KCl, and 1 mM $CaCl_2$) with or without 4 μM Fluo-4AM and 0.02% Pluronic F-127 for 1 h at 37 °C. The fresh assay buffer was added, and the cells were imaged at 20× and 60× on a Nikon Ti-E inverted confocal microscope equipped with an Andor CSU-X1 spinning disc and Andor DU-888 EM-CCD camera. For representative images, a single wide-field or confocal plane was selected, 30 s of the baseline signal was recorded, then the stimulation buffer (133 mM NaCl, 10 mM HEPES pH 7.4, 10 mM glucose, 7.5 mM KCl, and 1 mM $CaCl_2$) was manually applied via a micropipette, and the signal was imaged for a total of 3 min.

Statistical Analysis. Electrophysiological data were analyzed using Clampfit 10 (Molecular Devices), Excel (Microsoft), and GraphPad Prism 9.0 (GraphPad Software, La Jolla, CA) and were presented as mean ± standard error of the mean (SEM) and statistically analyzed with one-way ANOVA with Dunnett's posthoc test. For fluorescence in vitro cell-based experiments, the fluorescence peak response was normalized to the baseline and 100% activation or inhibition %, corresponding to its experimental settings. The normalized data were fit to a four-parameter logistic equation to determine the minimum response, maximum response (% E_{max}), the concentration giving the half-maximal response (EC_{50} or IC_{50}), and the slope factor of the curve using Origin 2018b (from OriginLab) or Prism 9.0.

■ ASSOCIATED CONTENT

Supporting Information

The Supporting Information is available free of charge at https://pubs.acs.org/doi/10.1021/acsptsci.1c00233.

Additional experimental details, materials, and methods (PDF)

■ AUTHOR INFORMATION

Corresponding Author

Jen Q. Pan − *Stanley Center for Psychiatric Research, Broad Institute of MIT and Harvard, Cambridge, Massachusetts 02142, United States*; Email: jpan@broadinstitute.org

Authors

Yan-Ling Zhang − *Stanley Center for Psychiatric Research, Broad Institute of MIT and Harvard, Cambridge, Massachusetts 02142, United States*

Sean P. Moran − *Stanley Center for Psychiatric Research, Broad Institute of MIT and Harvard, Cambridge, Massachusetts 02142, United States*; orcid.org/0000-0001-7672-242X

Andrew Allen − *Stanley Center for Psychiatric Research, Broad Institute of MIT and Harvard, Cambridge, Massachusetts 02142, United States*

David Baez-Nieto − *Stanley Center for Psychiatric Research, Broad Institute of MIT and Harvard, Cambridge, Massachusetts 02142, United States*

Qihong Xu − *Stanley Center for Psychiatric Research, Broad Institute of MIT and Harvard, Cambridge, Massachusetts 02142, United States*

Lei A. Wang − *Stanley Center for Psychiatric Research, Broad Institute of MIT and Harvard, Cambridge, Massachusetts 02142, United States*

William E. Martenis − *Stanley Center for Psychiatric Research, Broad Institute of MIT and Harvard, Cambridge, Massachusetts 02142, United States*

Joshua R. Sacher − *Stanley Center for Psychiatric Research, Broad Institute of MIT and Harvard, Cambridge, Massachusetts 02142, United States*

Jennifer P. Gale − *Stanley Center for Psychiatric Research, Broad Institute of MIT and Harvard, Cambridge, Massachusetts 02142, United States*

Michel Weïwer − *Stanley Center for Psychiatric Research, Broad Institute of MIT and Harvard, Cambridge, Massachusetts 02142, United States*; orcid.org/0000-0002-4897-1450

Florence F. Wagner − *Stanley Center for Psychiatric Research, Broad Institute of MIT and Harvard, Cambridge, Massachusetts 02142, United States*

Complete contact information is available at: https://pubs.acs.org/10.1021/acsptsci.1c00233

Author Contributions

Y.-L.Z. and S.P.M. contributed equally. Y.-L.Z. and J.Q.P. designed the study. S.P.M., D.B.Z., A.A., Q.X., J.G., J.S., L.A.W., and W.E.M. performed electrophysiological, cellular, and biochemical experiments and analyses. J.S., M.W., and F.F.W. provided chemistry support and compound information. S.P.M. and J.Q.P. wrote the manuscript. All the authors edited and reviewed the manuscript.

Notes

The authors declare no competing financial interest.

■ ACKNOWLEDGMENTS

The current work was supported by the following grants: R01 MH115045 (to J.Q.P.), U54 NS108874 (to J.Q.P.), R01

MH118298 (J.Q.P.) and the Stanley Center for Psychiatric Research.

ABBREVIATIONS

CHO, Chinese hamster ovary
CNS, central nervous system
EC_{50}, half-maximal effective concentration
FLIPR, fluorescence imaging plate reader
HEK, human embryonic kidney
IC_{50}, half-maximal inhibitory concentration
K_{ir}, inward rectifying potassium
LPA, lysophosphatidic acid
VGCCs, voltage-gated calcium channels

REFERENCES

(1) Simms, B. A.; Zamponi, G. W. Neuronal voltage-gated calcium channels: structure, function, and dysfunction. *Neuron* **2014**, *82*, 24−45.
(2) Zamponi, G. W.; Striessnig, J.; Koschak, A.; Dolphin, A. C. The Physiology, Pathology, and Pharmacology of Voltage-Gated Calcium Channels and Their Future Therapeutic Potential. *Pharmacol. Rev.* **2015**, *67*, 821−870.
(3) Magee, J. C.; Johnston, D. Characterization of single voltage-gated Na+ and Ca2+ channels in apical dendrites of rat CA1 pyramidal neurons. *J. Physiol.* **1995**, *487*, 67−90.
(4) Magee, J.; Hoffman, D.; Colbert, C.; Johnston, D. Electrical and calcium signaling in dendrites of hippocampal pyramidal neurons. *Annu. Rev. Physiol.* **1998**, *60*, 327−346.
(5) Ghosh, A.; Greenberg, M. E. Calcium signaling in neurons: molecular mechanisms and cellular consequences. *Science* **1995**, *268*, 239−247.
(6) Dunlap, K.; Luebke, J. I.; Turner, T. J. Exocytotic Ca2+ channels in mammalian central neurons. *Trends Neurosci.* **1995**, *18*, 89−98.
(7) Komuro, H.; Rakic, P. Selective role of N-type calcium channels in neuronal migration. *Science* **1992**, *257*, 806−809.
(8) Perez-Reyes, E. Molecular physiology of low-voltage-activated t-type calcium channels. *Physiol. Rev.* **2003**, *83*, 117−161.
(9) Ertel, E. A.; Campbell, K. P.; Harpold, M. M.; Hofmann, F.; Mori, Y.; Perez-Reyes, E.; Schwartz, A.; Snutch, T. P.; Tanabe, T.; Birnbaumer, L.; Tsien, R. W.; Catterall, W. A. Nomenclature of voltage-gated calcium channels. *Neuron* **2000**, *25*, 533−535.
(10) Catterall, W. A. Voltage-gated calcium channels. *Cold Spring Harbor Perspect. Biol.* **2011**, *3*, a003947.
(11) Dolphin, A. C. A short history of voltage-gated calcium channels. *Br. J. Pharmacol.* **2006**, *147*, S56−S62.
(12) Perez-Reyes, E. Molecular characterization of a novel family of low voltage-activated, T-type, calcium channels. *J. Bioenerg. Biomembr.* **1998**, *30*, 313−318.
(13) Bean, B. P. Neurotransmitter inhibition of neuronal calcium currents by changes in channel voltage dependence. *Nature* **1989**, *340*, 153−156.
(14) Fox, A. P.; Nowycky, M. C.; Tsien, R. W. Single-channel recordings of three types of calcium channels in chick sensory neurones. *J. Physiol.* **1987**, *394*, 173−200.
(15) Bean, B. P. Two kinds of calcium channels in canine atrial cells. Differences in kinetics, selectivity, and pharmacology. *J. Gen. Physiol.* **1985**, *86*, 1−30.
(16) Bean, B. P. Classes of calcium channels in vertebrate cells. *Annu. Rev. Physiol.* **1989**, *51*, 367−384.
(17) Weiss, N.; Zamponi, G. W. Genetic T-type calcium channelopathies. *J. Med. Genet.* **2020**, *57*, 1−10.
(18) Morino, H.; Matsuda, Y.; Muguruma, K.; Miyamoto, R.; Ohsawa, R.; Ohtake, T.; Otobe, R.; Watanabe, M.; Maruyama, H.; Hashimoto, K.; Kawakami, H. A mutation in the low voltage-gated calcium channel CACNA1G alters the physiological properties of the channel, causing spinocerebellar ataxia. *Mol. Brain* **2015**, *8*, 89.
(19) Barresi, S.; Dentici, M. L.; Manzoni, F.; Bellacchio, E.; Agolini, E.; Pizzi, S.; Ciolfi, A.; Tarnopolsky, M.; Brady, L.; Garone, G.; Novelli, A.; Mei, D.; Guerrini, R.; Capuano, A.; Pantaleoni, C.; Tartaglia, M. Infantile-Onset Syndromic Cerebellar Ataxia and CACNA1G Mutations. *Pediatr. Neurol.* **2020**, *104*, 40−45.
(20) Ernst, W. L.; Zhang, Y.; Yoo, J. W.; Ernst, S. J.; Noebels, J. L. Genetic Enhancement of Thalamocortical Network Activity by Elevating 1G-Mediated Low-Voltage-Activated Calcium Current Induces Pure Absence Epilepsy. *J. Neurosci.* **2009**, *29*, 1615−1625.
(21) Chemin, J.; Siquier-Pernet, K.; Nicouleau, M.; Barcia, G.; Ahmad, A.; Medina-Cano, D.; Hanein, S.; Altin, N.; Hubert, L.; Bole-Feysot, C.; Fourage, C.; Nitschké, P.; Thevenon, J.; Rio, M.; Blanc, P.; Vidal, C.; Bahi-Buisson, N.; Desguerre, I.; Munnich, A.; Lyonnet, S.; Boddaert, N.; Fassi, E.; Shinawi, M.; Zimmerman, H.; Amiel, J.; Faivre, L.; Colleaux, L.; Lory, P.; Cantagrel, V. De novo mutation screening in childhood-onset cerebellar atrophy identifies gain-of-function mutations in the CACNA1G calcium channel gene. *Brain* **2018**, *141*, 1998−2013.
(22) Calhoun, J. D.; Hawkins, N. A.; Zachwieja, N. J.; Kearney, J. A. Cacna1gis a genetic modifier of epilepsy caused by mutation of voltage-gated sodium channelScn2a. *Epilepsia* **2016**, *57*, e103−e107.
(23) Cain, S. M.; Tyson, J. R.; Choi, H.-B.; Ko, R.; Lin, P. J. C.; LeDue, J. M.; Powell, K. L.; Bernier, L.-P.; Rungta, R. L.; Yang, Y.; Cullis, P. R.; O'Brien, T. J.; MacVicar, B. A.; Snutch, T. P. CaV 3.2 drives sustained burst-firing, which is critical for absence seizure propagation in reticular thalamic neurons. *Epilepsia* **2018**, *59*, 778−791.
(24) Snutch, T. P.; Zamponi, G. W. Recent advances in the development of T-type calcium channel blockers for pain intervention. *Br. J. Pharmacol.* **2018**, *175*, 2375−2383.
(25) El Ghaleb, Y.; Schneeberger, P. E.; Fernández-Quintero, M. L.; Geisler, S. M.; Pelizzari, S.; Polstra, A. M.; van Hagen, J. M.; Denecke, J.; Campiglio, M.; Liedl, K. R.; Stevens, C. A.; Person, R. E.; Rentas, S.; Marsh, E. D.; Conlin, L. K.; Tuluc, P.; Kutsche, K.; Flucher, B. E. CACNA1I gain-of-function mutations differentially affect channel gating and cause neurodevelopmental disorders. *Brain* **2021**, *144*, 2092−2106.
(26) Mullins, M. E. Life-Threatening Interaction of Mibefradil and β-Blockers With Dihydropyridine Calcium Channel Blockers. *JAMA, J. Am. Med. Assoc.* **1998**, *280*, 157.
(27) Santi, C. M.; Cayabyab, F. S.; Sutton, K. G.; McRory, J. E.; Mezeyova, J.; Hamming, K. S.; Parker, D.; Stea, A.; Snutch, T. P. Differential inhibition of T-type calcium channels by neuroleptics. *J. Neurosci.* **2002**, *22*, 396−403.
(28) Powell, K. L.; Cain, S. M.; Snutch, T. P.; O'Brien, T. J. Low threshold T-type calcium channels as targets for novel epilepsy treatments. *Br. J. Clin. Pharmacol.* **2014**, *77*, 729−739.
(29) Singh, T.; Poterba, T.; Curtis, D.; Akil, H.; Al Eissa, M.; Barchas, J. D.; Bass, N.; Bigdeli, T. B.; Breen, G.; Bromet, E. J.; Buckley, P. F.; Bunney, W. E.; Bybjerg-Grauholm, J.; Byerley, W. F.; Chapman, S. B.; Chen, W. J.; Churchhouse, C.; Craddock, N.; Curtis, C.; Cusick, C. M.; DeLisi, L.; Dodge, S.; Escamilla, M. A.; Eskelinen, S.; Fanous, A. H.; Faraone, S. V.; Fiorentino, A.; Francioli, L.; Gabriel, S. B.; Gage, D.; Gagliano Taliun, S. A.; Ganna, A.; Genovese, G.; Glahn, D. C.; Grove, J.; Hall, M.-H.; Hamalainen, E.; Heyne, H. O.; Holi, M.; Hougaard, D. M.; Howrigan, D. P.; Huang, H.; Hwu, H.-G.; Kahn, R. S.; Kang, H. M.; Karczewski, K.; Kirov, G.; Knowles, J. A.; Lee, F. S.; Lehrer, D. S.; Lescai, F.; Malaspina, D.; Marder, S. R.; McCarroll, S. A.; Medeiros, H.; Milani, L.; Morley, C. P.; Morris, D. W.; Mortensen, P. B.; Myers, R. M.; Nordentoft, M.; O'Brien, N. L.; Olivares, A. M.; Ongur, D.; Ouwehand, W. H.; Palmer, D. S.; Paunio, T.; Quested, D.; Rapaport, M. H.; Rees, E.; Rollins, B.; Satterstrom, F. K.; Schatzberg, A.; Scolnick, E.; Scott, L.; Sharp, S. I.; Sklar, P.; Smoller, J. W.; Sobell, J. l.; Solomonson, M.; Stevens, C. R.; Suvisaari, J.; Tiao, G.; Watson, S. J.; Watts, N. A.; Blackwood, D. H.; Borglum, A.; Cohen, B. M.; Corvin, A. P.; Esko, T.; Freimer, N. B.; Glatt, S. J.; Hultman, C. M.; McQuillin, A.; Palotie, A.; Pato, C. N.; Pato, M. T.; Pulver, A. E.; St. Clair, D.; Tsuang, M. T.; Vawter, M. P.; Walters, J. T.; Werge, T.; Ophoff, R. A.; Sullivan, P. F.; Owen, M. J.; Boehnke,

https://doi.org/10.1021/acsptsci.1c00233
ACS Pharmacol. Transl. Sci. 2022, 5, 156−168

M.; O'Donovan, M.; Neale, B. M.; Daly, M. J. Exome Sequencing Identifies Rare Coding Variants in 10 Genes Which Confer Substantial Risk for Schizophrenia, **2020**, medRxiv.
(30) Andrade, A.; Hope, J.; Allen, A.; Yorgan, V.; Lipscombe, D.; Pan, J. Q. A rare schizophrenia risk variant of CACNA1I disrupts CaV3.3 channel activity. *Sci. Rep.* **2016**, *6*, 34233.
(31) Ghoshal, A.; Uygun, D. S.; Yang, L.; McNally, J. M.; Lopez-Huerta, V. G.; Arias-Garcia, M. A.; Baez-Nieto, D.; Allen, A.; Fitzgerald, M.; Choi, S.; Zhang, Q.; Hope, J. M.; Yan, K.; Mao, X.; Nicholson, T. B.; Imaizumi, K.; Fu, Z.; Feng, G.; Brown, R. E.; Strecker, R. E.; Purcell, S. M.; Pan, J. Q. Effects of a patient-derived de novo coding alteration of CACNA1I in mice connect a schizophrenia risk gene with sleep spindle deficits. *Transl. Psychiatry* **2020**, *10*, 29.
(32) Hawrylycz, M. J.; Lein, E. S.; Guillozet-Bongaarts, A. L.; Shen, E. H.; Ng, L.; Miller, J. A.; van de Lagemaat, L. N.; Smith, K. A.; Ebbert, A.; Riley, Z. L.; Abajian, C.; Beckmann, C. F.; Bernard, A.; Bertagnolli, D.; Boe, A. F.; Cartagena, P. M.; Chakravarty, M. M.; Chapin, M.; Chong, J.; Dalley, R. A.; Daly, B. D.; Dang, C.; Datta, S.; Dee, N.; Dolbeare, T. A.; Faber, V.; Feng, D.; Fowler, D. R.; Goldy, J.; Gregor, B. W.; Haradon, Z.; Haynor, D. R.; Hohmann, J. G.; Horvath, S.; Howard, R. E.; Jeromin, A.; Jochim, J. M.; Kinnunen, M.; Lau, C.; Lazarz, E. T.; Lee, C.; Lemon, T. A.; Li, L.; Li, Y.; Morris, J. A.; Overly, C. C.; Parker, P. D.; Parry, S. E.; Reding, M.; Royall, J. J.; Schulkin, J.; Sequeira, P. A.; Slaughterbeck, C. R.; Smith, S. C.; Sodt, A. J.; Sunkin, S. M.; Swanson, B. E.; Vawter, M. P.; Williams, D.; Wohnoutka, P.; Zielke, H. R.; Geschwind, D. H.; Hof, P. R.; Smith, S. M.; Koch, C.; Grant, S. G. N.; Jones, A. R. An anatomically comprehensive atlas of the adult human brain transcriptome. *Nature* **2012**, *489*, 391−399.
(33) Gadotti, V. M.; Kreitinger, J. M.; Wageling, N. B.; Budke, D.; Diaz, P.; Zamponi, G. W. Cav3.2 T-type calcium channels control acute itch in mice. *Mol. Brain* **2020**, *13*, 119.
(34) Nam, G. T-type calcium channel blockers: a patent review (2012-2018). *Expert Opin. Ther. Pat.* **2018**, *28*, 883−901.
(35) Hansen, K. B.; Bräuner-Osborne, H. FLIPR assays of intracellular calcium in GPCR drug discovery. *Methods Mol. Biol.* **2009**, *552*, 269−278.
(36) Zhu, T.; Fang, L.-y.; Xie, X. Development of a universal high-throughput calcium assay for G-protein-coupled receptors with promiscuous G-protein Gα15/16. *Acta Pharmacol. Sin.* **2008**, *29*, 507−516.
(37) Yu, H.-b.; Li, M.; Wang, W.-p.; Wang, X.-l. High throughput screening technologies for ion channels. *Acta Pharmacol. Sin.* **2016**, *37*, 34−43.
(38) Belardetti, F.; Tringham, E.; Eduljee, C.; Jiang, X.; Dong, H.; Hendricson, A.; Shimizu, Y.; Janke, D. L.; Parker, D.; Mezeyova, J.; Khawaja, A.; Pajouhesh, H.; Fraser, R. A.; Arneric, S. P.; Snutch, T. P. A fluorescence-based high-throughput screening assay for the identification of T-type calcium channel blockers. *Assay Drug Dev. Technol.* **2009**, *7*, 266−280.
(39) Pan, J. Q.; Baez-Nieto, D.; Allen, A.; Wang, H.-R.; Cottrell, J. R. Developing High-Throughput Assays to Analyze and Screen Electrophysiological Phenotypes. *Methods Mol. Biol.* **2018**, *1787*, 235−252.
(40) Kirkton, R. D.; Bursac, N. Engineering biosynthetic excitable tissues from unexcitable cells for electrophysiological and cell therapy studies. *Nat. Commun.* **2011**, *2*, 300.
(41) Heady, T. N.; Gomora, J. C.; Macdonald, T. L.; Perez-Reyes, E. Molecular pharmacology of T-type Ca2+ channels. *Jpn. J. Pharmacol.* **2001**, *85*, 339−350.
(42) Chen, T.-W.; Wardill, T. J.; Sun, Y.; Pulver, S. R.; Renninger, S. L.; Baohan, A.; Schreiter, E. R.; Kerr, R. A.; Orger, M. B.; Jayaraman, V.; Looger, L. L.; Svoboda, K.; Kim, D. S. Ultrasensitive fluorescent proteins for imaging neuronal activity. *Nature* **2013**, *499*, 295−300.
(43) Gao, J.; Liao, J.; Yang, G. Y. CAAX-box protein, prenylation process and carcinogenesis. *Am. J. Transl. Res.* **2009**, *1*, 312−325.
(44) Wang, M.; Casey, P. J. Protein prenylation: unique fats make their mark on biology. *Nat. Rev. Mol. Cell Biol.* **2016**, *17*, 110−122.
(45) Moriguchi, S.; Shioda, N.; Yamamoto, Y.; Tagashira, H.; Fukunaga, K. The T-type voltage-gated calcium channel as a molecular target of the novel cognitive enhancer ST101: enhancement of long-term potentiation and CaMKII autophosphorylation in rat cortical slices. *J. Neurochem.* **2012**, *121*, 44−53.
(46) Yabuki, Y.; Matsuo, K.; Izumi, H.; Haga, H.; Yoshida, T.; Wakamori, M.; Kakei, A.; Sakimura, K.; Fukuda, T.; Fukunaga, K. Pharmacological properties of SAK3, a novel T-type voltage-gated Ca2+ channel enhancer. *Neuropharmacology* **2017**, *117*, 1−13.
(47) Xu, J.; Yabuki, Y.; Yu, M.; Fukunaga, K. T-type calcium channel enhancer SAK3 produces anti-depressant-like effects by promoting adult hippocampal neurogenesis in olfactory bulbectomized mice. *J. Pharmacol. Sci.* **2018**, *137*, 333−341.
(48) Husain, N.; Yabuki, Y.; Shinoda, Y.; Fukunaga, K. Acute Treatment with T-Type Calcium Channel Enhancer SAK3 Reduces Cognitive Impairments Caused by Methimazole-Induced Hypothyroidism Via Activation of Cholinergic Signaling. *Pharmacology* **2018**, *101*, 309−321.
(49) Izumi, H.; Shinoda, Y.; Saito, T.; Saido, T. C.; Sato, K.; Yabuki, Y.; Matsumoto, Y.; Kanemitsu, Y.; Tomioka, Y.; Abolhassani, N.; Nakabeppu, Y.; Fukunaga, K. The Disease-modifying Drug Candidate, SAK3 Improves Cognitive Impairment and Inhibits Amyloid beta Deposition in App Knock-in Mice. *Neuroscience* **2018**, *377*, 87−97.
(50) Xie, X.; Van Deusen, A. L.; Vitko, I.; Babu, D. A.; Davies, L. A.; Huynh, N.; Cheng, H.; Yang, N.; Barrett, P. Q.; Perez-Reyes, E. Validation of High Throughput Screening Assays Against Three Subtypes of Cav3 T-Type Channels Using Molecular and Pharmacologic Approaches. *Assay Drug Dev. Technol.* **2007**, *5*, 191−204.
(51) Ohkubo, T.; Yamazaki, J.; Kitamura, K. Tarantula toxin ProTx-I differentiates between human T-type voltage-gated Ca2+ Channels Cav3.1 and Cav3.2. *J. Pharmacol. Sci.* **2010**, *112*, 452−458.
(52) Bladen, C.; Hamid, J.; Souza, I. A.; Zamponi, G. W. Block of T-type calcium channels by protoxins I and II. *Mol. Brain* **2014**, *7*, 36.
(53) Holdsworth, G.; Slocombe, P.; Hutchinson, G.; Milligan, G. Analysis of endogenous S1P and LPA receptor expression in CHO-K1 cells. *Gene* **2005**, *350*, 59−63.
(54) Riaz, A.; Huang, Y.; Johansson, S. G-Protein-Coupled Lysophosphatidic Acid Receptors and Their Regulation of AKT Signaling. *Int. J. Mol. Sci.* **2016**, *17*, 215.
(55) Swaney, J. S.; Chapman, C.; Correa, L. D.; Stebbins, K. J.; Broadhead, A. R.; Bain, G.; Santini, A. M.; Darlington, J.; King, C. D.; Baccei, C. S.; Lee, C.; Parr, T. A.; Roppe, J. R.; Seiders, T. J.; Ziff, J.; Prasit, P.; Hutchinson, J. H.; Evans, J. F.; Lorrain, D. S. Pharmacokinetic and pharmacodynamic characterization of an oral lysophosphatidic acid type 1 receptor-selective antagonist. *J. Pharmacol. Exp. Ther.* **2011**, *336*, 693−700.
(56) Klos, A.; Wende, E.; Wareham, K. J.; Monk, P. N. International Union of Basic and Clinical Pharmacology. LXXXVII. Complement Peptide C5a, C4a, and C3a Receptors. *Pharmacol. Rev.* **2013**, *65*, 500−543.
(57) Lohman, R.-J.; Hamidon, J. K.; Reid, R. C.; Rowley, J. A.; Yau, M.-K.; Halili, M. A.; Nielsen, D. S.; Lim, J.; Wu, K.-C.; Loh, Z.; Do, A.; Suen, J. Y.; Iyer, A.; Fairlie, D. P. Exploiting a novel conformational switch to control innate immunity mediated by complement protein C3a. *Nat. Commun.* **2017**, *8*, 351.
(58) Perez-Reyes, E. Molecular characterization of T-type calcium channels. *Cell. Calcium* **2006**, *40*, 89−96.
(59) Dana, H.; Sun, Y.; Mohar, B.; Hulse, B. K.; Kerlin, A. M.; Hasseman, J. P.; Tsegaye, G.; Tsang, A.; Wong, A.; Patel, R.; Macklin, J. J.; Chen, Y.; Konnerth, A.; Jayaraman, V.; Looger, L. L.; Schreiter, E. R.; Svoboda, K.; Kim, D. S. High-performance calcium sensors for imaging activity in neuronal populations and microcompartments. *Nat. Methods* **2019**, *16*, 649−657.
(60) Lee, J.; Song, K.; Lee, K.; Hong, J.; Lee, H.; Chae, S.; Cheong, E.; Shin, H.-S. Sleep spindles are generated in the absence of T-type calcium channel-mediated low-threshold burst firing of thalamocortical neurons. *Proc. Natl. Acad. Sci. U. S. A.* **2013**, *110*, 20266−20271.
(61) Candelas, M.; Reynders, A.; Arango-Lievano, M.; Neumayer, C.; Fruquière, A.; Demes, E.; Hamid, J.; Lemmers, C.; Bernat, C.; Monteil, A.; Compan, V.; Laffray, S.; Inquimbert, P.; Le Feuvre, Y.;

https://doi.org/10.1021/acsptsci.1c00233
ACS Pharmacol. Transl. Sci. 2022, 5, 156−168

Zamponi, G. W.; Moqrich, A.; Bourinet, E.; Méry, P.-F. Cav3.2 T-type calcium channels shape electrical firing in mouse Lamina II neurons. *Sci. Rep.* **2019**, *9*, 3112.
(62) Ly, R.; Bouvier, G.; Schonewille, M.; Arabo, A.; Rondi-Reig, L.; Lena, C.; Casado, M.; De Zeeuw, C. I.; Feltz, A. T-type channel blockade impairs long-term potentiation at the parallel fiber-Purkinje cell synapse and cerebellar learning. *Proc. Natl. Acad. Sci. U. S. A.* **2013**, *110*, 20302−20307.
(63) Pan, J.; Allen, A.; huang, L.; Daez, D. Characterizing rare missense variations of CACNA1I identified in a Swedish schizophrenia cohort. *Eur. Psychiatry* **2016**, *33*, S182−S183.
(64) Schneider, G. Automating drug discovery. *Nat. Rev. Drug Discovery* **2018**, *17*, 97−113.
(65) Wassermann, A. M.; Camargo, L. M.; Auld, D. S. Composition and applications of focus libraries to phenotypic assays. *Front. Pharmacol.* **2014**, *5*, 164.
(66) Kraus, R. L.; Li, Y.; Gregan, Y.; Gotter, A. L.; Uebele, V. N.; Fox, S. V.; Doran, S. M.; Barrow, J. C.; Yang, Z.-Q.; Reger, T. S.; Koblan, K. S.; Renger, J. J. In vitro characterization of T-type calcium channel antagonist TTA-A2 and in vivo effects on arousal in mice. *J. Pharmacol. Exp. Ther.* **2010**, *335*, 409−417.
(67) Tewson, P. H.; Quinn, A. M.; Hughes, T. E. A Multiplexed Fluorescent Assay for Independent Second-Messenger Systems. *J. Biomol. Screening* **2013**, *18*, 797−806.
(68) Raphemot, R.; Lonergan, D. F.; Nguyen, T. T.; Utley, T.; Lewis, L. M.; Kadakia, R.; Weaver, C. D.; Gogliotti, R.; Hopkins, C.; Lindsley, C. W.; Denton, J. S. Discovery, Characterization, and Structure?Activity Relationships of an Inhibitor of Inward Rectifier Potassium (Kir) Channels with Preference for Kir2.3, Kir3.X, and Kir7.1. *Front. Pharmacol.* **2011**, *2*, 75.
(69) Kim, N.; Shin, S.; Bae, S. W. cAMP Biosensors Based on Genetically Encoded Fluorescent/Luminescent Proteins. *Biosensors* **2021**, *11*, 39.
(70) Liu, C.-H.; Chen, Z.; Oliva, M. K.; Luo, J.; Collier, S.; Montell, C.; Hardie, R. C. Rapid Release of Ca2+ from Endoplasmic Reticulum Mediated by Na+/Ca2+ Exchange. *J. Neurosci.* **2020**, *40*, 3152−3164.
(71) Suzuki, J.; Kanemaru, K.; Iino, M. Genetically encoded fluorescent indicators for organellar calcium imaging. *Biophys. J.* **2016**, *111*, 1119−1131.
(72) McCue, H. V.; Wardyn, J. D.; Burgoyne, R. D.; Haynes, L. P. Generation and characterization of a lysosomally targeted, genetically encoded Ca2+-sensor. *Biochem. J.* **2013**, *449*, 449−457.
(73) Heyne, H. O.; Baez-Nieto, D.; Iqbal, S.; Palmer, D. S.; Brunklaus, A.; May, P.; Johannesen, K. M.; Lauxmann, S.; Lemke, J. R.; Møller, R. S.; Pérez-Palma, E.; Scholl, U. I.; Syrbe, S.; Lerche, H.; Lal, D.; Campbell, A. J.; Wang, H. R.; Pan, J.; Daly, M. J. Predicting functional effects of missense variants in voltage-gated sodium and calcium channels. *Sci. Transl. Med.* **2020**, *12*, No. eaay6848.

https://doi.org/10.1021/acsptsci.1c00233
ACS Pharmacol. Transl. Sci. 2022, 5, 156−168